IJBPAS, April, 2023, 12(4): 1452-1461

ISSN: 2277–4998

International Journal of Biology, Pharmacy and Allied Sciences (IJBPAS)

'A Bridge Between Laboratory and Reader'

www.ijbpas.com

SYNTHESIS AND CHARACTERIZATION OF TIN OXIDE NANOPARTICLES BY SIMPLE COST EFFECTIVE METHOD

PRASANNA MARY A AND SILAMBARASAN J*

Department of Chemistry, Theivanai Ammal College for Women (A), Villupuram, Tamil Nadu, India

***Corresponding Author: Dr. J. Silambarasan: E Mail: j.silambarasan@gmail.com**

Received 8th May 2022; Revised 16th June 2022; Accepted 27th Aug. 2022; Available online 1st April 2023

https://doi.org/10.31032/IJBPAS/2023/12.4.7009

ABSTRACT

The present study illustrates the characteristics and simple chemical method in a cost effective way for synthesis of tin oxide nanoparticles. The tin oxide nanoparticles were synthesized by using tin chloride, trichloroethylene and ortho phosphoric acid precipitators. Structure, size and surface morphology of the tin oxide was studied by X-ray diffraction (XRD), Fourier transform infrared spectroscopy (FTIR) and scanning electron microscopy (SEM). From the SEM, EDS and XRD analyses it can be concluded that, the synthesized SnO2 is rod shaped with average crystallite size ranging from 4 to 173 nm.

INTRODUCTION

Tin oxide is one of the most important versatile materials **[1]** owing to its high unit of transparency in the visible spectrum, strong physical and chemical interaction with adsorbed species, low operating temperature and strong thermal stability in air (up to 500 °C) **[2]**. Due to its two oxidation states +2 and +4, tin has two types of oxides that is stannous oxide (SnO) and stannic oxide (SnO_2), in which more stable is SnO_2 with a wide direct band gap (3.6 eV at 300 K). It has many applications like gas sensors, optoelectronic devices and negative electrodes for lithium batteries **[2-4]** due to high surface to volume ratio, compared to bulk tin oxide, which results in increased sensitivity and adsorption. Though, its sensing and electrical properties are to a large degree influenced by many factors. Depends upon the preparation method, SnO_2

size will be varied. Many methods have been established to synthesize SnO_2 nanoparticles, including low-temperature evaporation **[5]**, homogeneous precipitation **[6]**, water-in-oil microemulsions **[7]**, microwave-assisted solution **[8]**, sol–gel route **[9-11]**, thermal decomposition **[12]**, gas phase condensation **[13]**, dual ion beam sputtering **[14]** and amorphous citrate route **[15]**. Nanocrystalline structures have been achieved by these techniques, eventhough often with a very high degree of agglomeration. Tin oxide nanoparticles have been prepared by physical and chemical methods. Due to inexpensive and easy to complete, chemical synthesize methods were prepared. In that methods, solvents play a crucial important role in the synthesis of tin oxide nanoparticles.

Hence in the present work, we report the synthesize of tin oxide nanoparticles by sol–gel method at neutral pH. As the nanoparticles synthesized in different annealed times and their effect on the structural and morphological properties were studied.

2. EXPERIMENTAL PROCEDURE

Materials

Tin chloride ($SnCl_2$, Merck 99 %) as starting material, trichloroethylene as surfactant, absolute HCl as a solvent, ortho phosphoric acid as precipitator were used to prepare tin oxide nanoparticles. All the solutions were prepared using double distilled water.

Synthesis of SnO_2 powder

To 0.5 M $SnCl_2$, 10 ml of HCl was added. The mixture was then heated until to get clear solution. To that clear solution, 25 ml of H_3PO_4 was added drop by drop. The solution was made up to 100 ml with double distilled H_2O and followed by continuously stirred for 3 hrs, at room temperature. After one hour slightly white precipitate formed. After three hour the white precipitate was formed completely. The solution was decanted and the product formed was washed with water and then ethanol. Finally it was filtered using Wattman filter paper and dried in hot air oven (or) in muffle furnace and the yield was noted. The same procedure was carried out at 20ºC and 40ºC. The same procedure was carried out for 0.4 M and 0.6 M concentration of $SnCl_2$ also at 20ºC, 30ºC and 40ºC.

Characterization studies

Infrared spectroscopy

The FT-IR spectrum of a SnO_2 was recorded on a Bruker IFS 66 VFT-IR spectrometer using KBr pelleting technique and the absorption frequencies are expressed in reciprocal centimeters (cm^{-1}).

SEM analysis

The surface morphology, porosity and nanostructure of alumina powder were studied by SEM photographs. SEM analysis were taken by using the model JEOL-JSM-35 LF (Fig) which possess an accelerating voltage range of 5-35 kV with the magnification of 10-1,80,000 times. SEM photographs for the present studies were taken at 25KV with the magnification of 1000 times.

Energy Dispersive X-ray spectroscopy

The elements present in the alumina powder was analyzed by energy dispersive X-ray spectrometer using AN 10000 X-ray analyzer of LZ-5 Link Analytical Limited, UK.

X-Ray Diffraction

The nanostructure, texture, crystal orientation, particle size were determined by XRD. X-ray diffractometer (Model PW 1710, Philips Co.) equipped with a carbon monochromator and an automated sample changer was used for all XRD measurements and XRD scans were obtained under the following conditions:

Specimens of 2mm thick slices mounted on plastic plate holders was performed. X-rays were produced by a copper target operated at 25kV and 30mA. In order to extract the Full Width at Half Maximum (FWHM), the K_α contribution was subtracted and the data was fitted to a Pearson function. (a generalized Lorentz function).

To obtain X-ray diffraction scans of the loose fibres, the fibres were mounted on a low-background sample plate, made from a single quartz crystal, cut 6^0 from the C-axis. Angular measurements were made over a 2θ range from 10^0 to 80^0 in 0.05^0 steps with a count time of 1 s/step.

3. RESULTS AND DISCUSSION

Characterization

IR spectral analysis

Figure 1 shows the IR spectrum of nanocrystalline SnO_2 powder. From the figure, it can be seen that peaks arise about wave number 4000 cm^{-1} – 400 cm^1 are owing to stretching mode of SnO_2. After the high-pressure treatment, the characteristic peak of SnO_2 shifted as of wave number 438 cm^{-1} to 451 cm^{-1}. The characteristic peaks of pure SnO_2 showed blue shift. This is may be described as follows. Peaks happened with blue shift show that high pressure may expand the samples crystallinity and condense the distance of crystal lattice, which causes the enhancing of the field effect of crystal and increasing the band vibration frequency.

Stretching frequency of Sn-O can be seen at 1011cm^{-1} appeared as broad bands. It

was shown that Sn-O absorption bands convert broad as particle size decreases. It is assumed that, when the particle size decreases, surface effects will be enhanced so that damping of surface mode absorption will increases and hence Sn-O absorption bands become broadened. Other observed O^- bands at 3447 cm^{-1} may be due to the O-H stretching of water molecules. Due to the stretching of adsorbed CO_2 molecules, a peak appeared between in the range of 1600-1700 cm^{-1}. The peak appear at 511cm^{-1} may be due to the P-O stretching which may be obtained from phosphoric acid which was used in the synthesis of SnO_2.

XRD analysis

The surface nanostructure and texture of the synthesized SnO_2 nanostructures were analysed by XRD. **Figure 2** shows the XRD pattern of synthesized SnO_2 nanorods before and after treatments. Sharp peaks are observed which indicate the synthesized SnO_2 is exists in nanocrystalline nature. The XRD parameters such as 2θ, d value, crystal size are shown in **Table 1**. From the table and fig. it can be inferred that the SnO_2 nanorods are having only one phase with different crystal sizes and planes.

The sharp peaks indicate that the products were well crystallized. The diffraction peaks were in good agreement with those given in the standard data (PCPDF, 79-0207) for SnO_2 and showed a good crystallinity. This means that, as the prepared materials were crystallized in a hexagonal rutile structure of SnO_2 with the mean crystallite size, d is in inverse proportion to the full width at half maximum β(d=0.89 λ /(βcosθ), indicating that, the initial grain size to decrease.

The mean crystallite size d, was measured from the XRD (D.MAX-YB, RIGAKU) peaks at a scanning rate of 5º/min based on Scherrer's equation

$$d = \frac{0.9\lambda}{\beta\cos\theta'}$$

where λ is the wavelength of the X-ray, θ is the diffraction angle, and β is the full width at half maximum. The size of the SnO_2 crystallites ranged from 4 to 173 nm and the average crystallite size is 74 nm.

Figure 2 Shows the XRD pattern of synthesized powder without heat treatment. From the sharp intenses peaks, it can be infered that the powder without heat treatment is composed of SnO predominantly and SnO_2 to a maximum extent. After heat treatment, the XRD pattern of SnO_2 is completely different **Figure 2** is the XRD pattern of synthesized powder after 5 hrs and 10 hrs heat treatment respectively. After heat treatment it can be seen from the figures that,

most of the SnO phases disappear and peaks corresponding to SnO_2 appear, which indicates that, the synthesized powder is composed of SnO predominantly before heat treatment and it contains SnO_2 predominantly after treatment. Also it can be inferred that the SnO is converted into SnO_2 after heat treatment.

Figure 3 shows the surface morphologies of the synthesized SnO_2 powder at three magnifications X1500(a), X3000(b) and X6000(c). From the SEM images, it can be observed that, the synthesized SnO_2 particles are having rod shape, with varying diameters ranging from 400-800 nm. It can be seen that, some of the rod shaped particles are agglomerated and appear as platelets or sheets. Form the size, shape and diameters of the particles, one can infer that, the synthesized SnO_2 powder is the agglomeration of nanorods. The nanostructure and size can be further confirmed by XRD studies.

Deformation area near the crystal grain boundary is seen. May be it was caused by squeezing between crystals. From **Figure (3)**, it can be seen that, the crystal lattice was distorted by the grain squeeze which reveals that, deformation always occurs around crystalline exterior.

EDX analysis

Figure 4 show the EDX spectrum of the synthesized SnO_2 nanorods. From the EDX analysis, it can be detected that, the peaks corresponding to the energies of 3.05, 3.45, 3.75, 3.8, 4.1 and 4.3 eV are representing the Sn atom and a peak at 0.6 KeV represents the oxygen atom. The compound comprises of 30% Sn and 20% O which shows that, the synthesized powder is SnO_2. The other peaks are arises from carbon coated Cu grid for placing sample powder. The peak owing to P may be obtained from the phosphoric acid which was used in the synthesis of SnO_2. The chloride peak may arise due to the trace amount of Cl^- arising from the $SnCl_2$. Moreover there are so many peaks corresponding to Sn which may be due to different oxidation states of Sn^{2+} and Sn^{4+}. So the compound may be composed of both stannous (SnO_2) and stannic oxide (SnO_2).

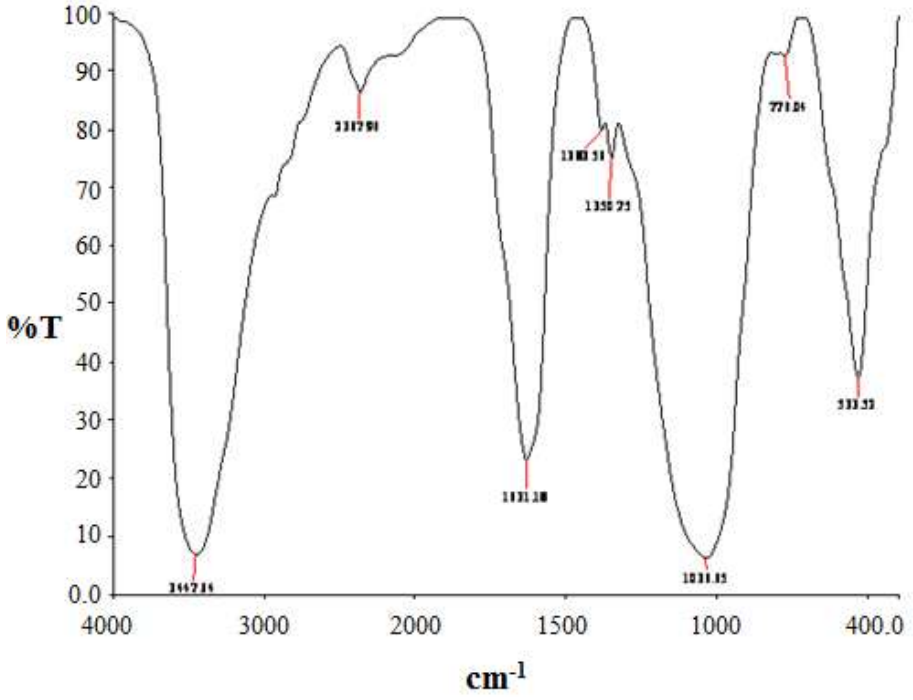

Figure 1: FT IR spectrum of SnO_2

Table 1: XRD Parameters of SnO_2 nanorods

Pos.[°2th.]	FWHM.[°2th.]	d-spacing.[A]	Rel. Int.[%]	Crystallite Size
12.8314	0.1775	6.8935	14.62	$9X10^{-9}$
20.2485	0.0929	4.3820	64.00	$173 X10^{-9}$
22.0071	0.1385	4.0357	19.37	$116 X10^{-9}$
22.8571	4.0000	3.8875	3.60	$4 X10^{-9}$
25.8883	0.1066	3.4388	100.00	$152 X10^{-9}$
28.1700	0.0992	3.1652	78.86	$165 X10^{-9}$
28.7493	0.1442	3.1027	44.86	$113 X10^{-9}$
29.7908	2.7514	2.9966	3.70	$5 X10^{-9}$
30.2651	2.1310	2.9507	3.79	$7 X10^{-9}$
31.2500	4.0000	2.8599	5.85	$4 X10^{-9}$
33.1293	0.1204	2.7018	91.02	$137 X10^{-9}$
36.0098	0.2337	2.4920	13.35	$71 X10^{-9}$
37.3898	1.5109	2.4032	3.0	$11 X10^{-9}$
38.6789	0.0982	2.3260	8.32	$171 X10^{-9}$
39.3316	0.5872	2.2889	7.84	$28 X10^{-9}$
44.8950	0.5094	2.0173	8.80	$33 X10^{-9}$
46.0314	0.1347	1.9701	26.54	$128 X10^{-9}$
51.2875	0.8751	1.7799	8.17	$20 X10^{-9}$

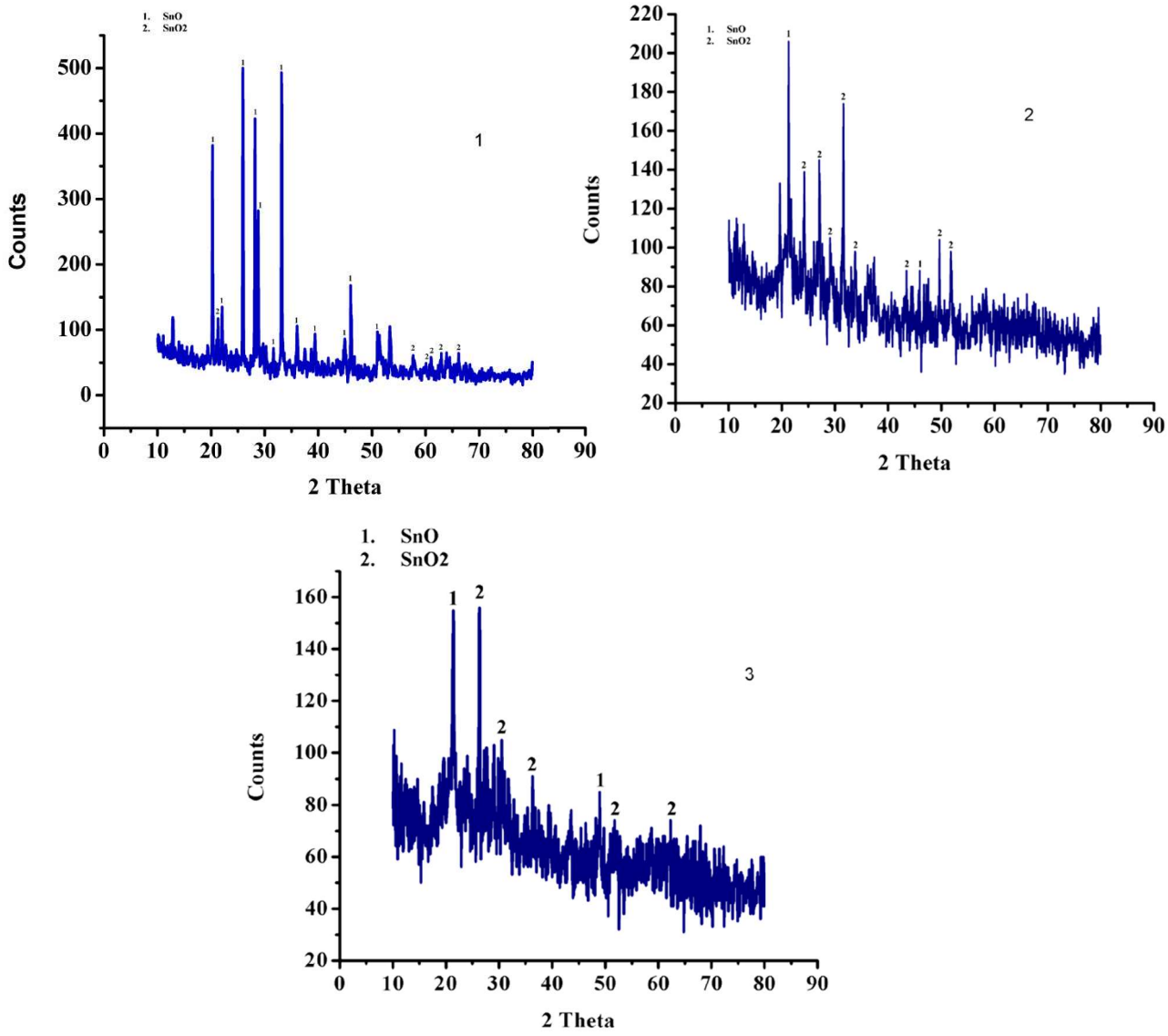

Figure 2: X-ray diffraction pattern of the SnO_2 before heat treatment and after 5 hrs and 10 hrs

Surface morphology

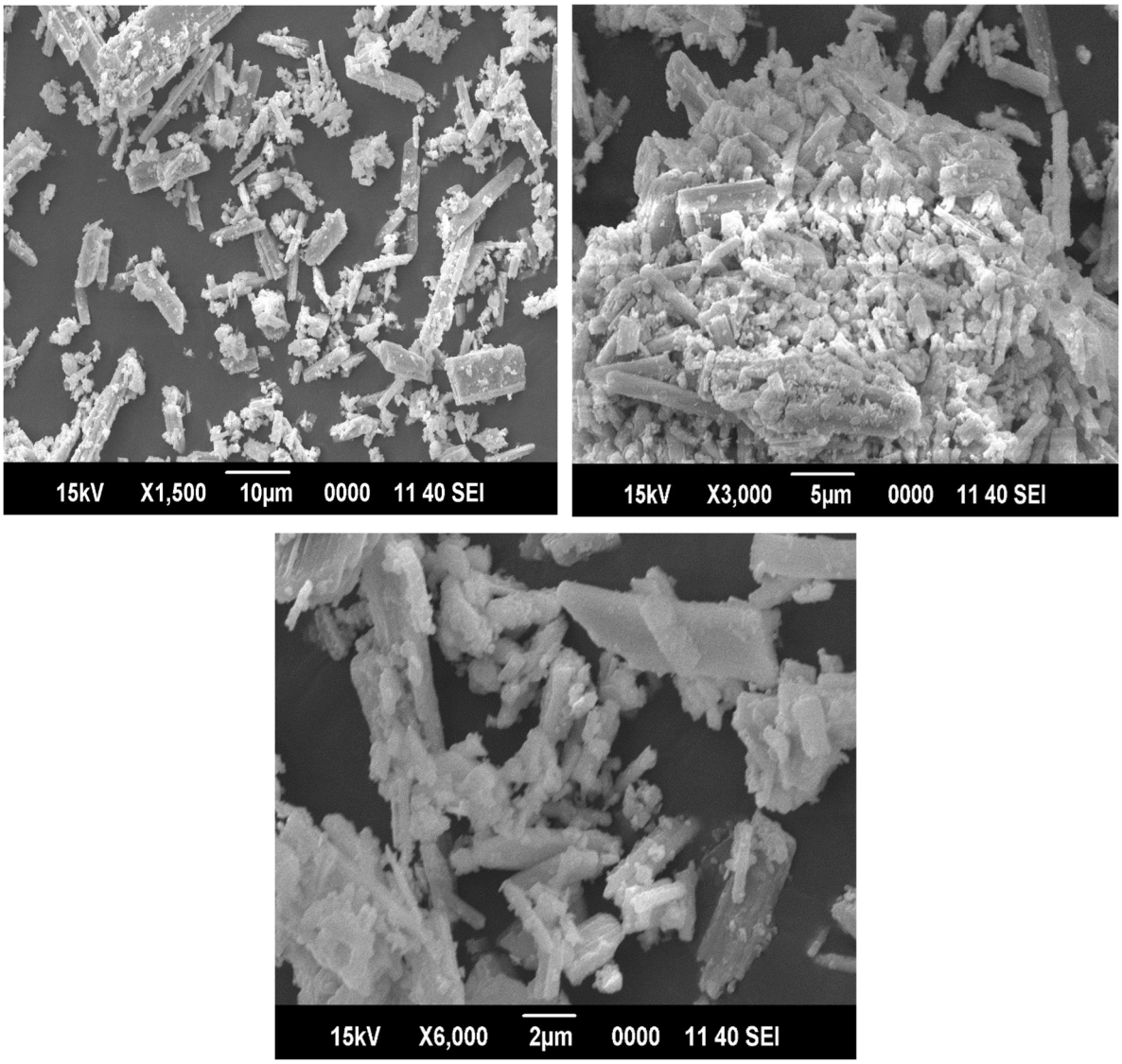

Figure 3: SEM image of SnO_2 with different magnification

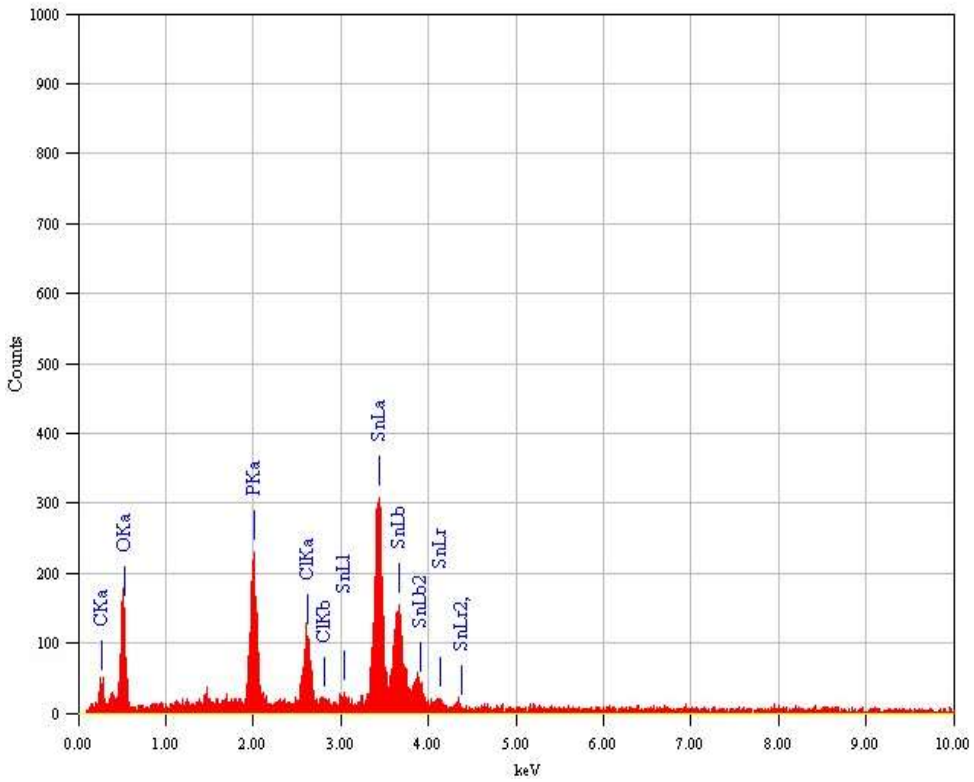

Figure 4: EDX spectrum of SnO_2 nanorods

CONCLUSIONS

Ultra-fine stannous oxide nanorods were synthesized by novel simple chemical method. The process parameters such as concentration of $SnCl_2$ phosphoric acid and HCl, stirring time, process temperature and other conditions were optimized to get ultra-fine nanorods. The nanostructure, surface morphology and size of the nanorods were studied by SEM and XRD. From the XRD, after heat treatment, most of the SnO phases disappear and SnO_2 peaks appear, which indicates that, the synthesized powder is composed of SnO predominantly before heat treatment and it contains SnO_2 predominantly after treatment. Sharp peaks are observed which indicate the synthesized SnO_2 is exists in nanocrystalline nature. The elemental composition was confirmed by EDX. In future, we are going to study the effect of corrosion inhibition and antimicrobial studies of as synthesized SnO_2 nanostructures.

REFERENCES

[1] Ge J.P., Wang J., Zhang H.X., Wang X., Peng Q., Li Y.D., Sensor Actuat. B-Chem., 113 (2006), 937.

[2] Adnan R., Razana N.A., Rahman I.A., Farrukh M.A., J. Chin. Chem. Soc.-TAIP, 57 (2010), 222.

[3] A.C. Bose, D. Kalpana, P. Thangadurai, S. Ramasamy, J. Power Sources 107 (2002) 138–141.

[4] F. Belliard, P.A. Connor, J.T.S. Irvine, Solid State Ionics 135 (2000) 163–167.

[5] F. Lu, Y. Liu, M. Dong, X. Wang, Sensors Actuators B 66 (2000) 225–227.

[6] Y. Chen, X. Cui, K. Zhang, D. Pan, Chem. Phys. Lett. 369 (2003) 16–20.

[7] K.C. Song, Y. Kang, Mater. Lett. 42 (2000) 283–289.

[8] K.C. Song, J.H. Kim, Powder Technol. 107 (2000) 268–272.

[9] D.S. Wu, C.Y. Han, S.Y. Wang, N.L. Wu, Mater. Lett. 53 (2002) 155–159.

[10] R. Pella, Sensors Actuators B 44 (1997) 462–467.

[11] A. Wilson, Sensors Actuators B 18/19 (1994) 506–510.

[12] H. Shiomi, C. Kakimoto, A. Nakakira, J. Sol-Gel Sci. Technol. 19 (2000) 759–763.

[13] C. Xu, G. Xu, Y. Liu, X. Zhao, Scripta Mater. 46 (2002) 789–794.

[14] J.-M. Herrmann, J. Disdier, A. Fernández, V.M. Jiménez, Nanostruct. Mater. 8 (1997) 675–686.

[15] Y.C. Choe, J.H. Chung, D.S. Kim, H.K. Baik, Surf. Coat. Technol. 112 (1999) 267–270.